arXiv:1401.0930v1 [physics.optics] 5 Jan 2014

# On phase-locking of Kerr combs

Aurélien Coillet[1,*] and Yanne Chembo[1]

[1] *FEMTO-ST Institute [CNRS UMR6174], Optics Department, 16 Route de Gray, 25030 Besançon cedex, France.*

compiled: January 7, 2014

We theoretically investigate the phase-locking phenomena between the spectral components of Kerr optical frequency combs in the dynamical regime of Turing patterns. We show that these Turing patterns display a particularly strong and robust phase-locking, originating from a cascade of phase-locked triplets which asymptotically lead to a global phase-locking between the modes. The local and global phase-locking relationship defining the shape of the optical pulses are analytically determined. Our analysis also shows that solitons display a much weaker phase-locking which can be destroyed more easily than in the Turing pattern regime. Our results indicate that Turing patterns are generally the most suitable for applications requiring the highest stability. Experimental generation of such combs is also discussed in detail, in excellent agreement with the numerical simulations.

*OCIS codes:* 140.3945,140.4050,190.4380,190.5530.
http://dx.doi.org/10.1364/XX.99.099999

Kerr optical frequency combs have been the focus of a strong interest from the scientific community since their first generation a few years ago [1]. These combs result from a four-wave mixing process, where new frequencies are generated through the nonlinear interaction between the light and the bulk material of a monolithic whispering-gallery mode (WGM) resonator. Depending on the frequency and power of the pump laser, this phenomenology leads to the excitation of equally spaced spectral lines, thereby forming the so-called Kerr comb. This multi-wavelength optical source is very promising for various applications such as high-resolution spectroscopy and ultra-stable microwave generation. In the latter case, the generated microwave corresponds to the beating between the different spectral modes, and its phase noise is directly related to the phase relationship between the comb's lines [2–4]. The understanding of the phase-locking process and its robustness with regard to external perturbations is therefore of the highest importance for ultra-stable microwave generation, and the objective of this letter is to unveil the mechanisms ensuring a stable and robust phase-locking between the modes.

The experimental setup used for Kerr comb generation is shown on Fig. 1. The output of a continuous-wave (CW) 1550 nm laser is amplified and coupled to an ultra-high $Q$ WGM resonator using the evanescent field of a tapered fiber. Above a given pump power threshold, a Kerr comb is generated and can be monitored using an optical spectrum analyzer.

* Corresponding author: aurelien.coillet@femto-st.fr

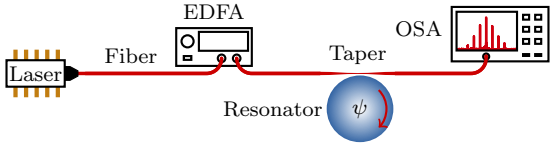


Fig. 1. Experimental setup.

A spatiotemporal formalism based on the Lugiato-Lefever equation (LLE) has recently been proposed to describe Kerr comb generation in WGM resonators [5–7]. In our case, the LLE can be writtten as [6]:

$$\frac{\partial\psi}{\partial\tau} = -(1+i\alpha)\psi + i|\psi|^2\psi - i\frac{\beta}{2}\frac{\partial^2\psi}{\partial\theta^2} + F \qquad (1)$$

where $\psi(\theta,\tau)$ is the complex amplitude of the overall field in the cavity, $\theta \in [-\pi,\pi]$ is the azimuthal angle along the cavity circumference, $\tau = t/2\tau_{\rm ph}$ is the normalized time, with $\tau_{\rm ph} = 1/\Delta\omega_{\rm tot}$ being the photon lifetime, $\Delta\omega_{\rm tot} = \omega_0/Q_{\rm tot}$ the loaded linewidth, and $Q_{\rm tot}$ the loaded quality factor. The parameter $\alpha = -2(\Omega-\omega_0)/\Delta\omega$ stands for the detuning between the pump laser and the cold resonance frequencies $\Omega$ and $\omega_0$, respectively. The parameter $\beta$ represents the second-order dispersion of the resonator, while $F$ stands for the amplitude of the pump laser field.

Various non-trivial solutions can emerge from the LLE depending on the parameters $\alpha$, $\beta$ and $F$ [8, 9]. In the regime of anomalous dispersion, the time-independent stationary solutions are either Turing patterns or bright solitons. In the spatio-temporal description, Turing patterns correspond to an integer number of intensity extrema along the azimuthal direction of the cavity. In the

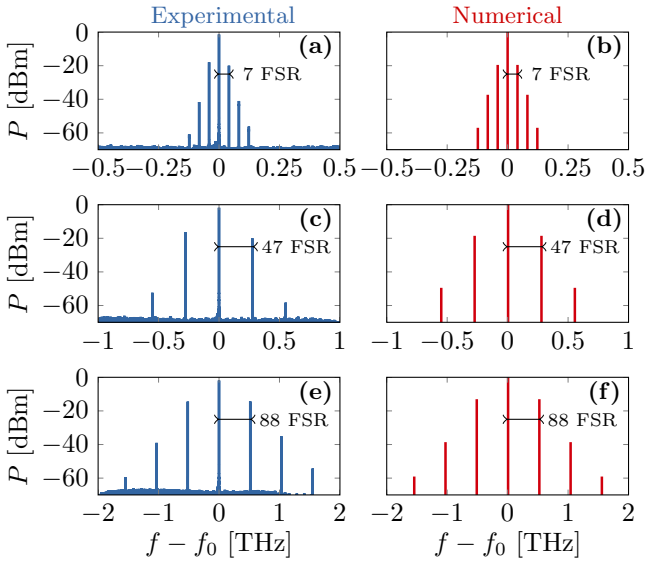


Fig. 2. Comparison between experimental (a, c and e) and theoretical (b, d and f) multiple-FSR spectra of Kerr combs corresponding to Turing patterns. Various line spacings are observed ranging from 7 to 88 FSR (41 to 516 GHz).

Fourier domain, these Turing patterns correspond to the well-known Kerr combs with multiple free-spectral range (FSR) spacing [10–13].

A few examples of such combs are presented in Fig. 2. They have been generated in a magnesium fluoride ($MgF_2$) resonator with intrinsic $Q$-factor equal to $1.5 \times 10^9$, and a FSR equal to $\Omega_{\mathrm{FSR}}/2\pi = 5.86$ GHz. By choosing different resonances, pump powers and frequencies, we were able to obtain different mode spacings, each corresponding to a different integer number of FSR [10]. For each one of these spectra, numerical simulations were performed using the split-step Fourier method on the LLE, and a good agreement with the experiments was found, hence validating the theoretical description. In the case of Fig. 2(b), the parameters used were $\beta = -0.03$, $\alpha = 1.27$ and $F^2 = 1.075$. For Fig. 2(d), $\beta$ is equal to $-0.003$, $\alpha = -1.3$ and $F^2 = 6.4$, while in Fig. 2(f), $\beta = -0.001$, $\alpha = -1.87$ and $F^2 = 14$.

In order to investigate theoretically the phase-locking of Turing patterns and their robustness relatively to solitons, an intermediate set-point was chosen, with $\beta = -0.03$, $\alpha = 0$, $F^2 = 2.5$ and noisy initial conditions, leading to the generation of the 12-th order Turing pattern shown in Fig. 3(a). Contrary to Turing patterns which fill entirely the cavity, the bright cavity soliton is a unique structure spinning in the cavity [13]. The spectrum of the soliton is therefore composed of spectral lines separated by only one FSR, as shown on Fig. 3(b) [$\alpha = 3$, $\beta = -0.03$, $F^2 = 3$; noisy Gaussian pulse initial condition]. Cavity solitons are known to be sub-critical dissipative structures, and in the LLE they appear for values of $\alpha$ greater than 41/30.

Turing patterns and cavity solitons are the two most

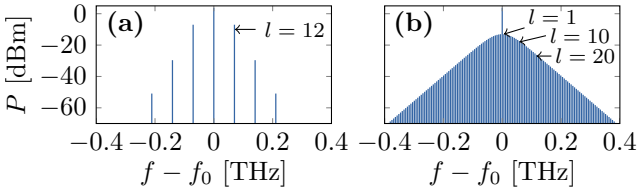


Fig. 3. Simulated spectra of: ($a$) A Turing pattern with $L = 12$. ($b$) A cavity soliton.

promising Kerr comb regimes for ultra-pure microwave generation. They are indeed structurally stable solutions of the LLE and can be obtained with parameters values far from chaotic regimes. In this application, the microwave signal corresponds to the beating between the different modes of the comb detected by a fast photodiode. In order to evaluate the phase properties of this beat-frequency, one needs to investigate the relative phases of the different modal components of the comb. From an analytical point of view, this task can hardly be performed using the LLE. Instead, the following modal decomposition

$$\psi(\theta,\tau) = \sum_l \Psi_l(\tau) e^{il\theta} \tag{2}$$

allows to have direct access to the phase $\varphi(\tau)$ of the slowly-varying modal amplitudes $\Psi_l = |\Psi_l| e^{i\varphi}$, with $l = \ell - \ell_0$ being the azimuthal eigennumber of the photons with respect to the pumped mode (the pumped mode is therefore $l = 0$, while the sidemodes correspond to $l = \pm 1, \pm 2, \dots$). By plugging the expansion of Eq. (2) inside the LLE, the following ordinary differential equations ruling the dynamics of each mode is obtained:

$$\frac{d\Psi_l}{d\tau} = \left[-(1+i\alpha) + i\frac{\beta}{2} l^2\right] \Psi_l + \delta(l)\, F + i \sum_{m,n,p} \delta(m-n+p-l)\, \Psi_m \Psi_n^* \Psi_p\,, \tag{3}$$

where $\delta(x)$ is the usual Kronecker function, while $m$, $n$, $p$, and $l$ are eigennumbers labelling the interacting modes following the interaction $\hbar\omega_m + \hbar\omega_p \leftrightarrow \hbar\omega_n + \hbar\omega_l$. It is important to note that strict equivalence between the modal and spatiotemporal models had been demonstrated in ref. [6], so that the theoretical analysis can be performed with either formalism depending on their specific advantages.

The regime of Turing pattern is essentially originating from modulational instability, which was analyzed in detail in refs. [11–15]. Turing patterns actually arise from the following cascade of interactions. When the pump is set above the threshold $F_{\mathrm{th}}^2 = 1 + (1-\alpha)^2$, the modes around $\pm l_{\mathrm{th}}$ with $l_{\mathrm{th}} = [(2(\alpha-2)/\beta)]^{1/2}$ experience positive gain and are thereby excited. After a transient dynamics characterized by modal competition, two symmetric sidemodes $\pm L \simeq \pm l_{th}$ are stabilized around the pump and the net flux of photons follows the degenerate interaction $2\hbar\omega_0 \rightarrow \hbar\omega_L + \hbar\omega_{-L}$.

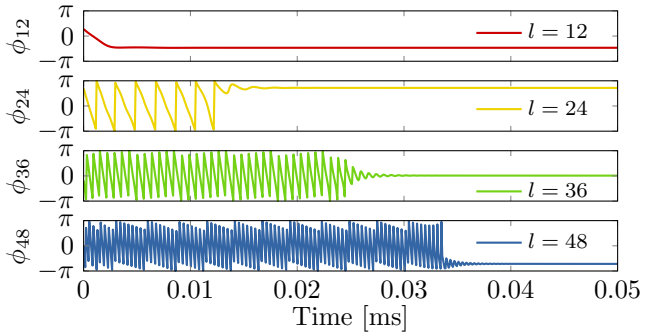


Fig. 4. Time evolution of the relative phases of the 4 first modes of the Turing pattern of Fig. 2(a). After a delay increasing with the mode number, the relative phases reach a constant value, the Kerr comb becoming phase-locked.

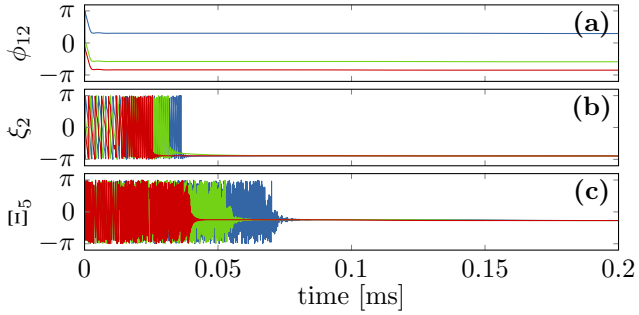


Fig. 5. Phase-locking behavior for different noisy initial conditions. (a) Phase difference $\phi_{12} = \varphi_{12} - \varphi_0$. Evidence of triplet phase-locking ((b), $\xi_2$ is constant) and global phase-locking ((c), $\Xi_5$ is constant).

From then, the sidemodes $\pm L$ provide in their turn a net flux of photons to the sidemodes $\pm 2L$ using interactions $\hbar\omega_0 + \hbar\omega_{\pm L} \rightarrow \hbar\omega_{\mp L} + \hbar\omega_{\pm 2L}$. This cascaded process is further generalized later through the interactions $\hbar\omega_0 + \hbar\omega_{\pm L} \rightarrow \hbar\omega_{\mp kL} + \hbar\omega_{\pm(k+1)L}$ where the sidemodes $\pm kL$ provide a net flux of photons to the sidemodes $\pm(k+1)L$. This cascaded fountain effect asymptotically yields a Kerr comb characterized by a multiple-FSR spacing of multiplicity $L$. The effect of this cascading mechanism can be observed in Fig. 4, displaying the phase dynamics of the 12-th order Turing patterns of Fig. 3(a). It can be clearly seen that after a transient dynamics, the various modal phases $\phi_l = \varphi_l - \varphi_0$ with respect to the pump are reaching a time-independent value. The phase stabilization occurs first for the mode $l = 12$, and then to $l = 24$, $l = 36$, and so on.

It is important to note that the phase locking value depends on the initial condition, as illustrated on Fig. 5(a), where the phase difference $\phi_l = \varphi_l - \varphi_0$ for $l = 12$ has been plotted for different initial conditions. This phenomenon is true for all the excited modes of the Turing pattern. However, it can be shown that an intrinsic phase-locking relationship takes place between the modes of the comb. According to the scenario described earlier, a given mode $kL$ mainly interacts with its two neighboring modes $(k \pm 1)L$. In the steady state ($d\Psi_{kL}/d\tau \equiv 0$), this three-mode interaction can be rewritten as

$$\begin{aligned}\kappa_{kL}\Psi_{kL} = \delta(k)\, F + |\Psi_{kL}|^2\Psi_{kL} \\ 2\{|\Psi_{(k-1)L}|^2\Psi_{kL} + |\Psi_{(k+1)L}|^2\Psi_{kL} \\ +\Psi_{(k-1)L}\Psi^*_{kL}\Psi_{(k+1)L}\}\end{aligned} \tag{4}$$

with $\kappa_l = -(1 + i\alpha) + i\beta l^2/2$. By extracting the phases in this relashionship, it appears that consecutive triplets of modes are necessarily phase-locked according to

$$\xi_k = \varphi_{(k-1)L} - 2\varphi_{kL} + \varphi_{(k+1)L} = \text{Constant}\,. \tag{5}$$

Hence, the phases $\varphi_{kL}$ might individually have an asymptotic value that depends on the initial conditions, but for the same Turing pattern, the combination $\varphi_{(k-1)L} - 2\varphi_{kL} + \varphi_{(k+1)L}$ will be *independent* of initial conditions and will converge to the same value $\xi_k$, as it can be seen in Fig. 5(b). The value of $\xi_k$ depends only on the parameters $\alpha$, $\beta$, $F$ and $k$. The sequence is therefore the following: initially, the triplet $\{-L, 0, L\}$ is the first to phase-lock. Then the two triplets $\{0, \pm L, \pm 2L\}$ phase lock, and later on, all the cascade of triplets $\{\pm(k-1)L, \pm kL, \pm(k+1)L\}$ as $k \rightarrow +\infty$ successively phase lock as well.

This sequence of triplet phase-locking ultimately leads to a global phase coupling through a cascaded process, and the global phase-locking relationship can be obtained by considering that since any $\xi_k$ is constant, so is any linear combination of them. In particular, if we consider $2N + 1$ oscillating modes in a Turing pattern comb (the pump and $N$ excited modes on each side), we can show that,

$$\begin{aligned}\Xi_N &= \frac{1}{2}\sum_{k=-(N-1)}^{k=N-1}\left[1 - (-1)^{N+k}\right]\xi_k \\ &= \varphi_{-NL} + 2\sum_{k=-(N-1)}^{k=N-1}(-1)^{N+k}\varphi_{kL} + \varphi_{NL} \\ &= \text{Constant}\,.\end{aligned} \tag{6}$$

If we consider for example the 7 oscillating modes that are visible in Fig. 3(a), this global phase locking relationship simply reads $\Xi_3 = \varphi_{-36} - 2\varphi_{-24} + 2\varphi_{-12} - 2\varphi_0 + 2\varphi_{12} - 2\varphi_{24} + \varphi_{36} = \text{Constant}$. This relationship can include more modes if needed [for example the modes $l = \pm 48$, which are indeed oscillating as it can be seen in Fig. 4(d)]. Hence, when the permanent state is reached, the linear combination $\Xi_N$ which involves all the modal phases is a constant that is independent of the initial conditions, as evidenced by Fig. 5(c). These intrinsic phase relations $\xi_k$ and $\Xi_N$ are therefore responsible for the shape of the Kerr comb in the Turing pattern regime.

In order to test the robustness of the phase-locking in both the Turing pattern and the soliton regimes, we introduce a perturbation after the stationary state is reached: the phase of the pump signal is abruptly

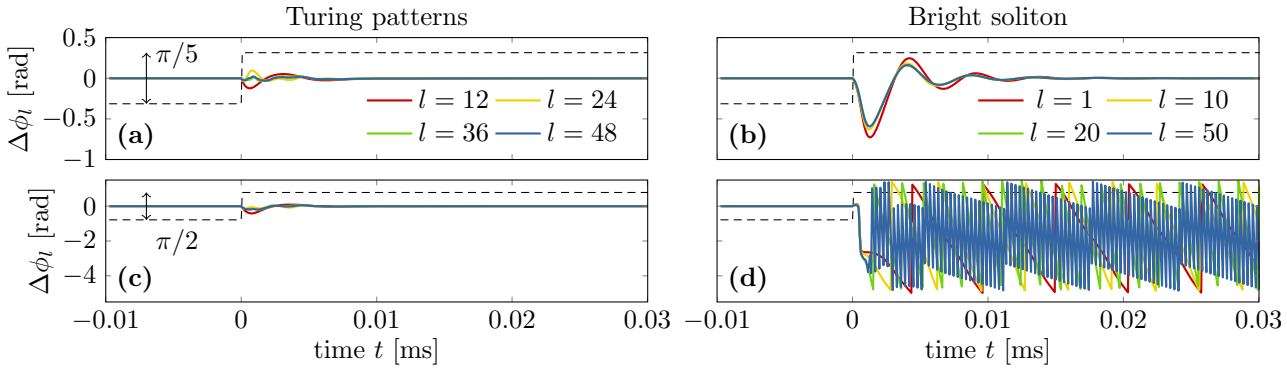


Fig. 6. Variation of the relative phases $\Delta\phi_l$ of different spectral modes of the Kerr combs while the pump signal undergoes an abrupt phase transition. (a) and (c): Case of the Turing pattern of Fig. 3(a). (b) and (d): Case of the bright soliton comb of Fig. 3(b). At $t = 0$, the phase of the pump is shifted by $\pi/5$ in (a) and (b) and by $\pi/2$ for (c) and (d). In the $\pi/5$ phase shift case, oscillations in the relative phases of the comb's lines are observed, but the phase-locking returns to its previous state and value. The amplitude and duration of these oscillations are much larger in the case of the bright soliton compared to the Turing patterns case. In the $\pi/2$ phase shift case, while the phase locking of the Turing pattern is maintained, the soliton is destroyed, and thus the phase locking.

shifted by constant offset, and we monitor the difference $\Delta\phi_l(t) = \phi_l(t) - \phi_l^{\mathrm{st}}$, with $\phi_l = \varphi_l - \varphi_0$. When the offset in the pump phase is set to $\pi/5$, the relative phases of the different modes oscillate in response to this perturbation, but the phase-locking is preserved. In the case of the Turing patterns, the phase oscillations are of small amplitude with respect to the perturbation, and decrease when the mode number increases, as if the perturbation was attenuated during its propagation to higher order modes. In contrast, the amplitudes of the phase oscillations of the soliton are larger than the initial stimulus, and do not substantially decrease for higher order modes. This result indicates that Turing patterns are more robust to external phase perturbations, and could lead to better phase-noise performances. To strengthen this claim, the phase-shift of the pump signal was increased to $\pi/2$, and the resulting phase evolution is plotted in Fig. 6(c) and (d). The Turing pattern behavior remains very stable and identically phase-locked, while the soliton is destroyed (as well as the phase-locking).

In this work we have given an insight into the dynamics of phase-locking in a Kerr frequency comb. The fact that the photonic interactions are strongly dominated by exchange of microwave photons of energy $L \times \hbar\Omega_{\mathrm{FSR}}$ is a direct consequence of the modulational instability, which generates the highest gain for photons whose offset frequency relatively to the pump is precisely $L \times \Omega_{\mathrm{FSR}}$. We have analytically demonstrated that phase-locking in Turing patterns is achieved through a cascaded phase-locking of adjacent triplets, which ultimately leads to a global phase-locking relationship that we have determined. We have also shown that Turing patterns are more robust than solitons with regards to external perturbations, thereby demonstrating their stronger potential for ultra-stable microwave generation.

Y. C. K. acknowledges financial support from the European Research Council (ERC) through the project NextPhase.

## References

[1] T. J. Kippenberg, R. Holzwarth, and S. A. Diddams, Science **332**, 555–559 (2011).
[2] P. Del'Haye, S. B. Papp, and S. A. Diddams, Phys. Rev. Lett. **109**, 263901 (2012).
[3] J. Li, H. Lee, T. Chen and K. Vahala, Phys. Rev. Lett. **109**, 233901 (2012).
[4] A. B. Matsko and L. Maleki, Opt. Express. **21**, 28862–28876 (2013).
[5] A. B. Matsko, A. A. Savchenkov, W. Liang, V. S. Ilchenko, D. Seidel, and L. Maleki, Opt. Lett. **36**, 2845–2847 (2011).
[6] Y. K. Chembo and C. R. Menyuk, Phys. Rev. A **87**, 053852 (2013).
[7] S. Coen, H. G. Randle, T. Sylvestre, and M. Erkintalo, Optics Letters **38**, 37–39 (2013).
[8] I. Balakireva, A. Coillet, C. Godey, and Y. K. Chembo, arXiv:1308.2542 (2013).
[9] C. Godey, I. Balakireva, A. Coillet, and Y. K. Chembo, arXiv:1308.2539 (2013).
[10] A. A. Savchenkov, A. B. Matsko, V. S. Ilchenko, I. Solomatine, D. Seidel, and L. Maleki, Phys. Rev. Lett. **101**, 093902 (2008).
[11] Y. K. Chembo, D. V. Strekalov, and N. Yu, Phys. Rev. Lett. **104**, 103902 (2010).
[12] Y. K. Chembo and N. Yu, Phys. Rev. A **82**, 033801 (2010).
[13] A. Coillet, I. Balakireva, R. Henriet, K. Saleh, L. Larger, J. Dudley, C. Menyuk, and Y. K. Chembo, Photonics Journal, IEEE **5**, 6100409 (2013).
[14] T. Hansson, D. Modotto, and S. Wabnitz, Phys. Rev. A **88**, 023819 (2013).
[15] M. R. E. Lamont, Y. Okawachi, and A. L. Gaeta, Opt. Lett. **38**, 3478–3481 (2013).

## References


[1] T. J. Kippenberg, R. Holzwarth, and S. A. Diddams, "Microresonator-Based Optical Frequency Combs," Science **332**, 555–559 (2011).

[2] P. Del'Haye, S. B. Papp, and S. A. Diddams, "Hybrid electro-optically modulated microcombs," Phys. Rev. Lett. **109**, 263901 (2012).

[3] J. Li, H. Lee, T. Chen and K. Vahala, "Low-pump-power, low-phase-noise and microwave to millimeter-wave repetition rate operation in microcombs," Phys. Rev. Lett. **109**, 233901 (2012).

[4] A. B. Matsko and L. Maleki, "On timing jitter jitter of mode locked Kerr frequency combs," Opt. Express. **21**, 28862–28876 (2013).

[5] A. B. Matsko, A. A. Savchenkov, W. Liang, V. S. Ilchenko, D. Seidel, and L. Maleki, "Mode-locked kerr frequency combs," Opt. Lett. **36**, 2845–2847 (2011).

[6] Y. K. Chembo and C. R. Menyuk, "Spatiotemporal lugiato-lefever formalism for kerr-comb generation in whispering-gallery-mode resonators," Phys. Rev. A **87**, 053852 (2013).

[7] S. Coen, H. G. Randle, T. Sylvestre, and M. Erkintalo, "Modeling of octave-spanning kerr frequency combs using a generalized mean-field lugiato-lefever model," Optics Letters **38**, 37–39 (2013).

[8] I. Balakireva, A. Coillet, C. Godey, and Y. K. Chembo, "Stability Analysis of the Lugiato-Lefever Model for Kerr Optical Frequency Combs. Part II: Case of Anomalous Dispersion," arXiv:1308.2542 `http://arxiv.org/abs/1308.2542` (2013).

[9] C. Godey, I. Balakireva, A. Coillet, and Y. K. Chembo, "Stability Analysis of the Lugiato-Lefever Model for Kerr Optical Frequency Combs. Part I: Case of Normal Dispersion," arXiv:1308.2539 `http://arxiv.org/abs/1308.2539` (2013).

[10] A. A. Savchenkov, A. B. Matsko, V. S. Ilchenko, I. Solomatine, D. Seidel, and L. Maleki, "Tunable optical frequency comb with a crystalline whispering gallery mode resonator," Phys. Rev. Lett. **101**, 093902 (2008).

[11] Y. K. Chembo, D. V. Strekalov, and N. Yu, "Spectrum and dynamics of optical frequency combs generated with monolithic whispering gallery mode resonators," Phys. Rev. Lett. **104**, 103902 (2010).

[12] Y. K. Chembo and N. Yu, "Modal expansion approach to optical-frequency-comb generation with monolithic whispering-gallery-mode resonators," Phys. Rev. A **82**, 033801 (2010).

[13] A. Coillet, I. Balakireva, R. Henriet, K. Saleh, L. Larger, J. Dudley, C. Menyuk, and Y. K. Chembo, "Azimuthal turing patterns, bright and dark cavity solitons in kerr combs generated with whispering-gallery-mode resonators," Photonics Journal, IEEE **5**, 6100409 (2013).

[14] T. Hansson, D. Modotto, and S. Wabnitz, "Dynamics of the modulational instability in microresonator frequency combs," Phys. Rev. A **88**, 023819 (2013).

[15] M. R. E. Lamont, Y. Okawachi, and A. L. Gaeta "Route to stabilized ultrabroadband microresonator-based frequency combs," Opt. Lett. **38**, 3478–3481 (2013).